Actuating and detecting of microdroplet using slanted finger interdigital transducers

Tsung-Tsong Wu[a] and I-Hsiang Chang
Institute of Applied Mechanics, National Taiwan University, Taipei 106, Taiwan

(Received 14 October 2004; accepted 20 May 2005; published online 20 July 2005)

Using surface acoustic wave (SAW) to drive droplets on a piezoelectric chip is a distinctive microfluidic technique developed recently. In the previous research, uniform interdigital transducers (IDTs) were used to radiate SAW amplitude and move the droplets within the same delay line simultaneously. In this paper, we employ slanted finger interdigital transducers (SFITs) to replace uniform IDTs. The merit is that we can move individual droplets at will by varying the frequency. This is because SAW amplitude profile actuated by a SFIT is not uniform along the aperture. The position of the maximum amplitude can be changed by adjusting the input frequency. In addition, we apply the coupling-of-modes model to simulate the amplitude profile and the frequency response of SFITs. Since the transmitted SAW intensity is strongly attenuated by the liquid when SAW hits the droplet, we can use the measured frequency response to detect the position of the droplet and verify the validity of the proposed method; we fabricated a SFIT on an Y128X-$LiNbO_3$ substrate coated with hydrophobic film. The experimental results show good agreement with those predicted by the simulations. We note that the proposed method can further be used to construct a multichannel microfluidic chip. © *2005 American Institute of Physics*. [DOI: 10.1063/1.1949710]

I. INTRODUCTION

In a surface acoustic wave (SAW) device, SAW is excited by interdigital electrodes on a piezoelectric substrate, resulting in the vibration of the surface. As SAW propagates along the interface between a liquid and a solid, it is transformed into leaky surface acoustic wave (LSAW) and the acoustic energy is radiated into the liquid[1,2] so that a body force and a pressure gradient are generated. If the gradient is large enough, an acoustic streaming will be induced to move a droplet forward, as shown in Fig. 1. An advantage of this method is that the droplets can be controlled efficiently by adjusting the input rf signal. However, the SAW amplitude excited by uniform interdigital transducers (IDTs) is the same throughout the aperture. If droplets are placed within the same delay line, not blocking one another, they will all be driven simultaneously.[3,4] In other words, the droplets cannot be controlled individually or sequentially for consequent chemical processes unless using many sets of uniform IDTs which will eventually lead to a complex configuration and arduous command of circuits.

It is known that the SAW amplitude excited by a slanted finger interdigital transducer (SFIT) is not uniform and different amplitude profiles can be agitated by changing the input frequency. Yatsuda[5] and Yatsuda *et al.*[6,7] used Smith's equivalent circuit and angular spectrum methods to get the amplitude profile of SFIT. He found that the former obtaining the electric potential by the equivalent circuit is an easier and faster method. The coupling-of-modes (COM) model has been used to simulate the frequency response of layered SAW device with uniform IDTs.[8,9] Recently, Wu and Lin used this model to analyze the frequency response of a SFIT.[10] On the experimental verification, the surface acoustic wave field of SFIT was measured in the experiments by Dufilie *et al.*[11] He used a scanning Michelson interferometer to obtain the SAW-field distribution and found out that a narrow acoustic main beam could be generated at designated position of the aperture by adjusting the input frequency. Toward the detection of position of a microdroplet, the fact that the transmitted SAW intensity is strongly attenuated by the liquid when SAW hits the droplet can be utilized.

In this paper, we used SFITs as the wave source to drive individual droplets. We use the COM model to simulate the performance of SFIT. To demonstrate the validity of the proposed multichannel concept, we fabricated a SFIT on an Y128X-$LiNbO_3$ substrate coated with a hydrophobic film. The results are in very good agreement with those predicted based on our simulations.

II. ANALYSIS OF SLANTED FINGER INTERDIGITAL TRANSDUCER

In this section, the displacement amplitude profile and the frequency response for detecting the position of the droplet are calculated based on the COM model,[12] In addition, the effects of the number of electrode pairs and the bandwidth of the optimum design of SFIT will be discussed.

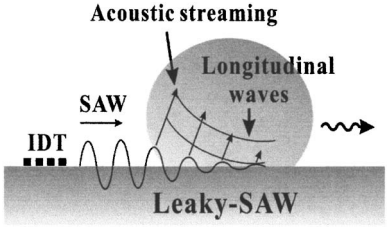

FIG. 1. Acoustic streaming used to drive a droplet.

[a]Author to whom correspondence should be addressed; Fax: (886) 2-33665665; electronic mail: wutt@ndt.iam.ntu.edu.tw

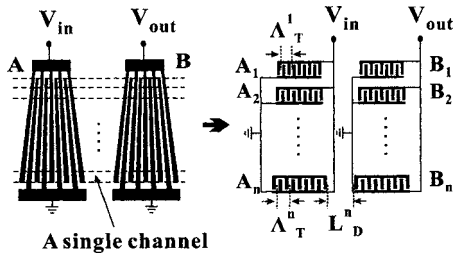

FIG. 2. Configuration of SFIT and its equivalent circuit.

A. Displacement amplitude profile

The displacement amplitude of the surface acoustic wave is proportional to the surface electric potential generated by the transducer. When a signal is inputted continuously at the center frequency of the transducer, the displacement excited from each electrode pair will be superposed. Owing to this relationship between the electric potential and displacement, we can use the admittance $|Y_{12}|$ to represent the amplitude profile radiated from the SFIT.[5,10]

In this paper, the method of equal aperture separations is introduced into the COM model to obtain Y_{12} of the SFIT.[10] In Fig. 2, a transmission is conceptually divided into n subfilters parallel to the propagation direction of the SAW. If n is large enough $(30 \leqslant n \leqslant 100)$, the tilt of the electrodes could be neglected. In other words, each subfilter can be approximated as filters with uniform finger width. We defined i as the number of the channel which is a single subfilter; thus, $\boldsymbol{A_i}$ and $\boldsymbol{B_i}$ are input and output ports in the ith transmission channel. The admittance elements of the $[\mathbf{Y}^i]$ matrix in one channel can be obtained from the $[\mathbf{P}^i]$ matrix[10] as

$$\begin{bmatrix} I_A^i \\ I_B^i \end{bmatrix} = \begin{bmatrix} Y_{11}^i & Y_{12}^i \\ Y_{21}^i & Y_{22}^i \end{bmatrix} \begin{bmatrix} V_A^i \\ V_B^i \end{bmatrix}, \tag{1}$$

$$Y_{11}^i = P_{33}^{A_i} + P_{11}^{B_i} \left[\frac{P_{32}^{A_i} P_{23}^{A_i}}{1 - P_{11}^{B_i} P_{22}^{A_i} e^{-i2kL_D^i}} \right] e^{-j2kL_D^i}, \tag{2}$$

$$Y_{12}^i = \frac{P_{32}^{A_i} P_{13}^{B_i}}{1 - P_{11}^{B_i} P_{22}^{A_i} e^{-j2kL_D^i}} e^{-jkL_D^i}, \tag{3}$$

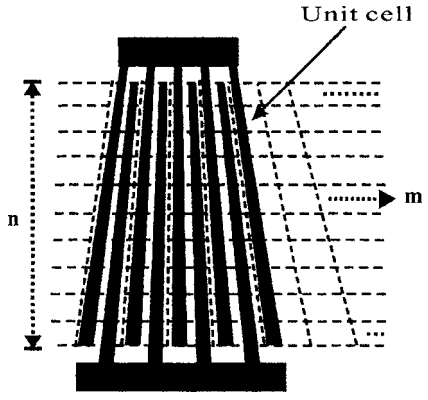

FIG. 3. Unit computational cells of a SFIT defined for simulation.

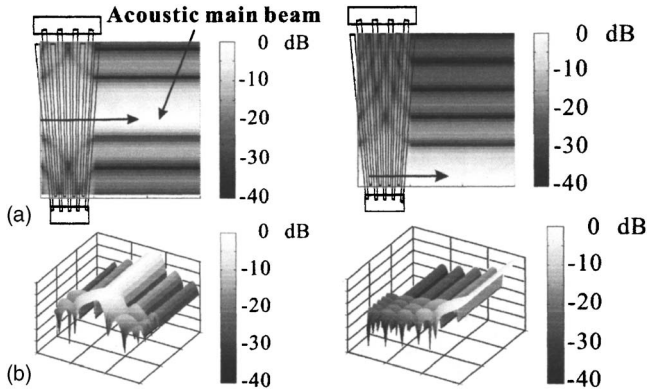

FIG. 4. Simulation results of the displacement field excited by SFIT with input signal of (a) 68 MHz and (b) 71.6 MHz. Logarithmic scale indicates the relative power of the acoustic wave. Power is proportional to amplitude of displacement, therefore the regions of 0 dB have the largest amplitude in the displacement field.

$$Y_{21}^i = \frac{P_{23}^{A_i} P_{31}^{B_i}}{1 - P_{11}^{B_i} P_{22}^{A_i} e^{-j2kL_D^i}} e^{-jkL_D^i}, \tag{4}$$

$$Y_{22}^i = P_{33}^{B_i} + P_{22}^{A_i} \left[\frac{P_{13}^{B_i} P_{31}^{B_i}}{1 - P_{11}^{B_i} P_{22}^{A_i} e^{-j2kL_D^i}} \right] e^{-j2kL_D^i}, \tag{5}$$

where I_A^i and I_B^i are the bus bar currents of the input port $\boldsymbol{A_i}$ and the output port $\boldsymbol{B_i}$, respectively. V_A^i is the electric potential of the input port $\boldsymbol{A_i}$ and V_B^i is that of the output port $\boldsymbol{B_i}$. $P_{xy}^{A_i}$ and $P_{xy}^{B_i}$ are the element of the $[\mathbf{P}^{A_i}]$ matrix and the $[\mathbf{P}^{B_i}]$ matrix, respectively.

In order to observe the whole displacement field of SFIT, each channel is divided into m cells, and the width of each cell is equal to the wavelength of the SAW which is excited from that channel, as shown in Fig. 3. When a continuous signal is given into the SFIT, the SAW amplitude exists in the right cell and is accumulated from the first left cell to that specific one in the same channel, and vice versa. Therefore, the amplitude of each cell can be represented by $|Y_{12}^{ij}|$, where j is defined as the number of the cell in one channel. We note that the SAW amplitude of the cell locating in the area of the electrodes should be calculated by adding both the acoustic wave propagating to the right, denoted by $Y_{12}^{ij(+)}$, and to the left, denoted by $Y_{12}^{i(m-j)(-)}$; hence, the $|Y_{12}^{ij}|$ for the cell ij is

$$|Y_{12}^{ij}| = |Y_{12}^{ij(+)}| + |Y_{12}^{i(m-j)(-)}|. \tag{6}$$

Figure 4 shows the simulated result of the displacement

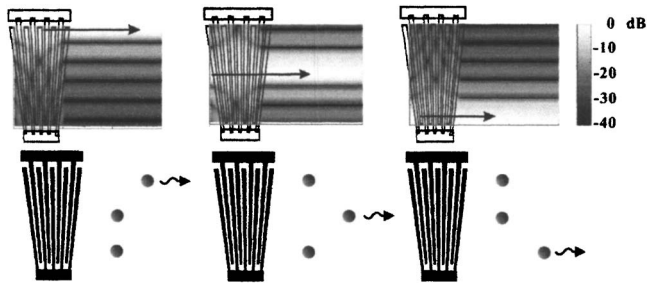

FIG. 5. Different input frequencies, (a) lower frequency, (b) center frequency, and (c) higher frequency, allow to drive droplets at different locations along a SFIT.

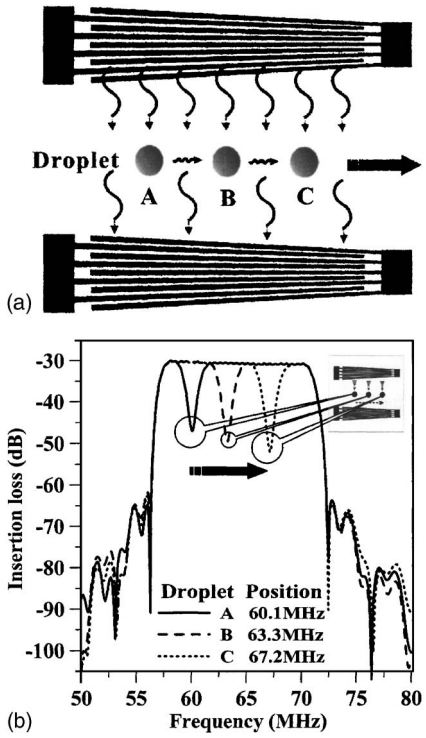

FIG. 6. Location of droplet can be determined by frequency response. Droplets at positions A, B, and C correspond to the drops of insertion loss at frequencies 60.1, 63.3, and 67.2 MHz, respectively.

amplitude on the substrate Y128X-$LiNbO_3$. The number of electrode pairs is 50 and the passband of the frequency response is between 64.6 and 71.6 MHz. The logarithmic scale indicates the relative power of the surface acoustic waves. The power is proportional to the displacement amplitude, so 0 dB represents the largest amplitude. When a signal is given at 68 MHz near the center frequency of the passband, the largest displacement amplitude is generated at the center of the aperture (the lightest area). We call this the acoustic main beam. The position of the acoustic main beam can be switched to the higher-frequency end ("lower" edge) of the SFIT when the frequency is raised to 71.6 MHz.

Since the amplitude of the acoustic main beam is largest in a SFIT. If sufficient electric power is used to induce the amplitude of the acoustic main beam pass a critical value, the droplet placed on the acoustic main beam will be moved. The droplets on the other acoustic beams where the amplitudes do not exceed the critical value will remain still. Furthermore, the position of the acoustic main beam can be changed with the input of different frequencies. This way, only the droplets on the desired position will be moved, as shown in Fig. 5.

B. Frequency response for detecting the positions of droplets

The variation of the finger period over the SFIT aperture generates a wide passband of frequency response. A single frequency within the passband corresponds to a single channel which transmits a relatively narrow SAW beam at the respective position in the SFIT. If a droplet is placed on some channel, the acoustic power of the SAW beam transmitting

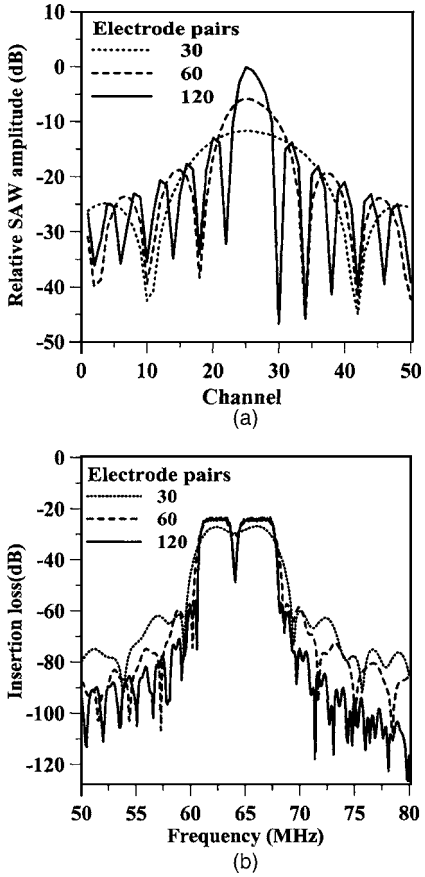

FIG. 7. Simulation results of (a) amplitude profiles; (b) frequency responses for detecting a droplet using a SFIT with different number of electrode pairs.

along that area will be absorbed by the droplet. This will cause the center frequency of that channel to have the maximum insertion loss within the passband. Therefore, the relative position of the droplet between two SFITs can be indicated according to the drop of frequency response within the passband.

We also use the COM model to simulate the frequency response. As the subfilters are connected in parallel, in Fig. 2, the bus bar current of a SFIT is the summation of all the channels. The admittance matrix $[\mathbf{Y}]$ of the SFIT can be represented as

$$\begin{bmatrix} I_A \\ I_B \end{bmatrix} = \begin{bmatrix} \sum Y_{11}^{ij} & \sum Y_{12}^{ij} \\ \sum Y_{21}^{ij} & \sum Y_{22}^{ij} \end{bmatrix} \begin{bmatrix} V_{\text{in}} \\ V_{\text{out}} \end{bmatrix} = \begin{bmatrix} Y_{11} & Y_{12} \\ Y_{21} & Y_{22} \end{bmatrix} \begin{bmatrix} V_{\text{in}} \\ V_{\text{out}} \end{bmatrix}. \tag{7}$$

All elements of the $[\mathbf{Y}^i]$ matrices of the channels where the droplet exists can be assumed as zero because the acoustic power is absorbed. Then the simulate frequency response for detecting the position of a droplet can be obtained by substituting the elements of the $[\mathbf{Y}]$ matrix into the equation presented as follows:

$$S_{21} = \frac{-2\sqrt{R_1 R_2}Y_{21}}{(1+Z_1Y_{11})(1+Z_2Y_{22}) - Y_{12}Y_{21}Z_1Z_2}, \tag{8}$$

where Z_1 and Z_2 are the input and output impedances, respectively. R_1 and R_2 are the real part of Z_1 and Z_2.

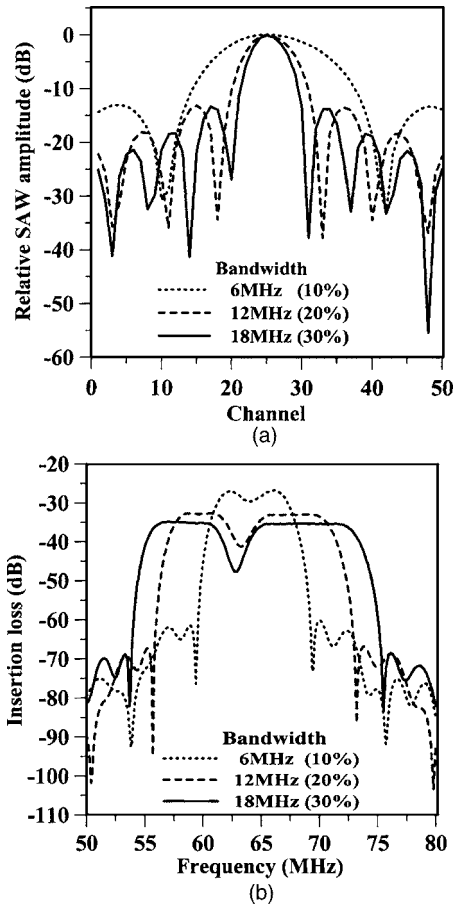

FIG. 8. Simulation results of (a) amplitude profiles; (b) frequency responses for detecting a droplet using a SFIT with different bandwidth.

The simulated results are shown in Fig. 6. In Fig. 6(a), the positions of a droplet moving forward can be detected by a SFIT, and we found that the positions of the droplets A, B, and C are indicated, respectively, at different frequencies, 60.1, 63.3, and 67.2 MHz, with higher insertion loss, as shown in Fig. 6(b).

C. Effects of parameters on the SFIT

In this section, the effects of the number of pairs of electrodes and the bandwidth are discussed in order to obtain designs with better performance for driving and detecting droplets. In Figs. 7(a) and 8(a), we focus only on the amplitude profile of the wave propagating in the delay line and illustrate it in two dimensions to compare the differences; in Figs. 7(b) and 8(b), we compare the frequency responses which show the position of the droplet. First, we define the ratio of the width of the droplet base to the aperture as 3/50.

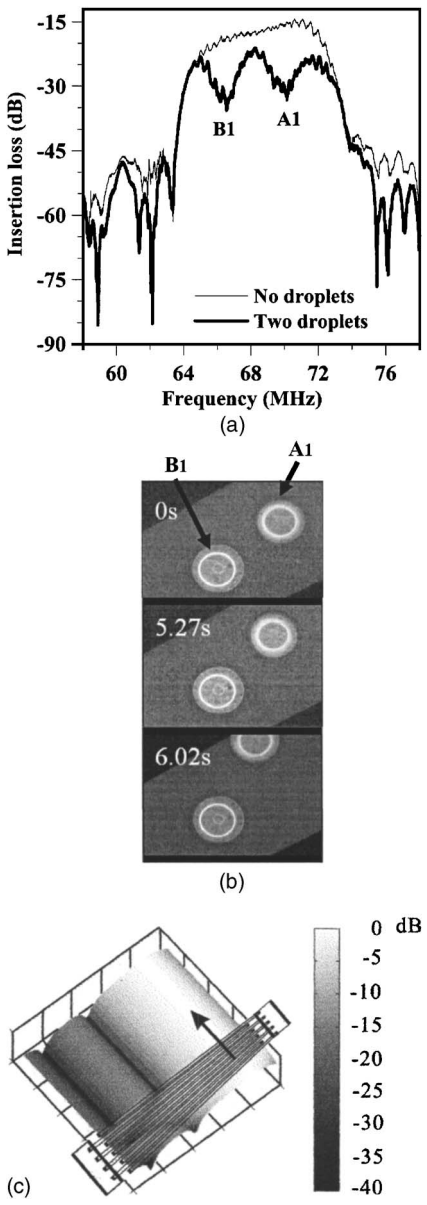

FIG. 9. (a) The frequency response which indicates the positions of the droplet A_1 and droplet B_1. Acoustic waves passing through the droplets have their energies absorbed by the droplets, resulting in a drop in insertion loss. The drops of insertion loss at frequencies 70.1 and 66.5 MHz can be used to pinpoint the locations of the droplet A_1 and droplet B_1 along the SFIT; (b) simulated result of displacement field caused by SFIT with input signal of 70.1 MHz [two 0.7-μl droplets were detected and driven by the SFIT (Design 3)].

The aperture is 2000 μm in the simulation. We use Y128X-$LiNbO_3$ as the substrate, so the Euler angles are 0°, 38°, and 90°. In addition, we assume that the droplets are placed on the central area of the delay line.

TABLE I. Parameters of the designed SFITs in the experiment.

Parameter	Bandwidth	λ_{min}	λ_{max}	Input and output pairs	Aperture	Propagation distance	Max. tilt angle	Euler angles
Unit	%	μm	μm	pairs	μm	μm	degree	degree
Design 1	10	54	60	30-20	4000	3407	1.3	(0, 38, 90)
Design 2	20	51.2	64	30-20	5000	3714	2.22	(0, 38, 90)
Design 3	10	54	60	30-20	4000	3407	1.3	(0, 38, 0)

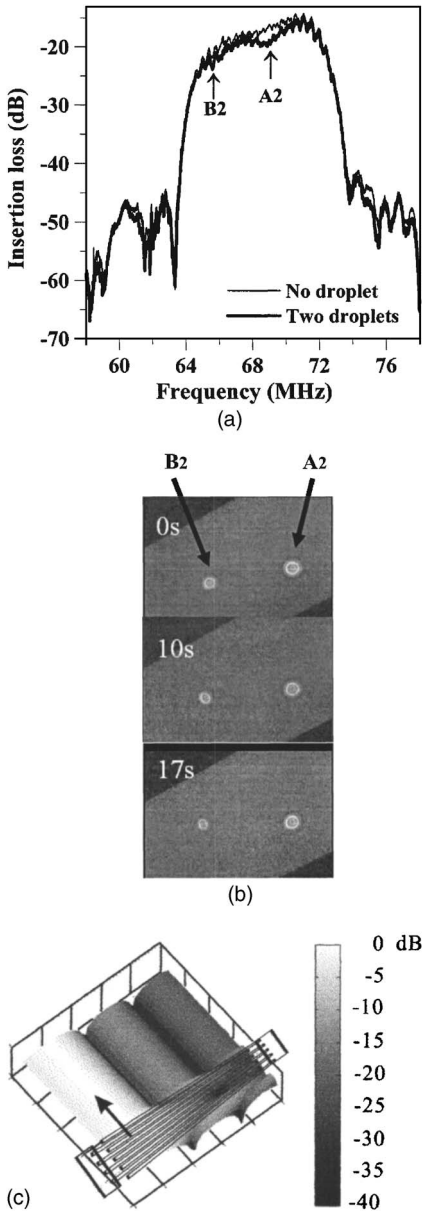

FIG. 10. (a) The frequency response which indicates the positions of the droplets A_2 and B_2. The frequencies with higher insertion loss, 69 and 65.6 MHz, represent the respective positions of the droplets; (b) images show the motion of the droplet driven by SFIT; (c) simulated result of displacement field at 65.6 MHz [two 0.1-μl droplets were detected and driven by the SFIT (Design 3)].

1. Number of electrode pairs

Figure 7(a) shows the amplitude profiles varying with different number of electrode pairs. By increasing the number of electrode pairs, the area of acoustic main beam becomes smaller and the amplitude becomes higher, allowing the droplet to be driven more easily. However, the amplitude will not continue to increase if the number of electrode pairs goes past 120. One advantage of smaller acoustic main beam is that we can control more individual droplets using the same SFIT, and by adding more electrode pairs we can use less electric power to drive the droplet. Furthermore, Fig. 7(b) shows that the passband of the frequency response is between 61.2 and 68 MHz. The frequency with maximum

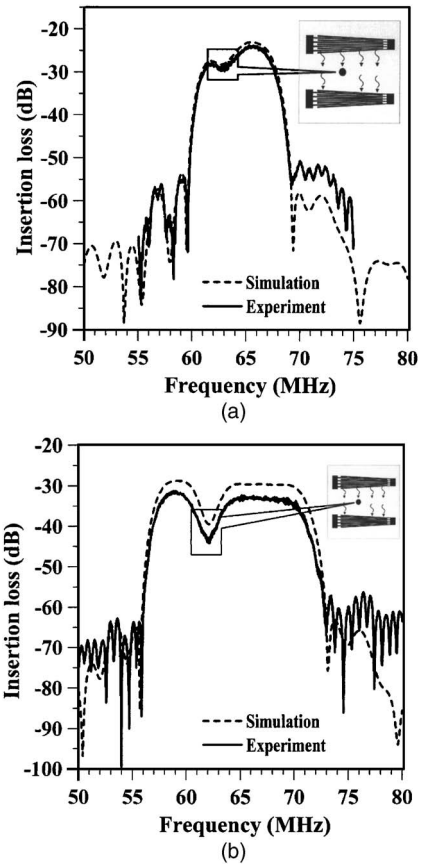

FIG. 11. Comparisons between the frequency responses of simulations and experimental results. (a) bandwidth: 10% (Design 1); (b) bandwidth: 20% (Design 2). The volume of the droplet was about 0.1 μl.

insertion loss in passband can be identified more easily using the SFIT with more electrode pairs, enhancing the sensitivity for detection the position of the droplet.

2. Bandwidth

In our experiments we selected bandwidths of 6, 12, and 18 MHz to study the influences of bandwidths on the acoustic main beams and amplitudes. From Fig. 8(a), it can be seen that the biggest bandwidth of 18 MHz results in the narrowest acoustic main beam. However, the amplitudes remain constant irregardless of the bandwidths used. Figure 8(b) shows that the sensitivity is improved by increasing the bandwidth. We conclude that increasing the electrode pairs or bandwidth results in an extremely narrow acoustic main beam with good sensitivity. However, the increase in the amplitude can only be achieved by increasing the number of electrode pairs. Varying the bandwidth will not help since it will only affect the width of the acoustic main beam.

In summary, our simulation shows that designs with more electrode pairs or larger bandwidth perform better in the identification of the positions of the droplets. It is worth noting that the design with more electrode pairs is recommended because it makes the efficiency of droplets driving higher.

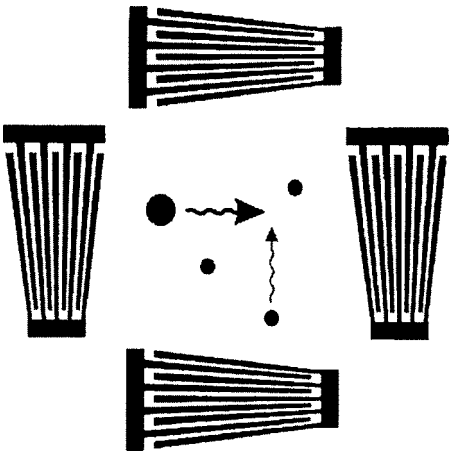

FIG. 12. Diagram of the multichannel microfluidic chip. SFIT can be used to mix different microdroplets that are inserted at different location.

III. FABRICATION OF THE SFITS AND THE HYDROPHOBIC FILM

The design parameters of the SFITs in our experiments are listed in Table I. Y128X-$LiNbO_3$ is selected as the substrate. After fabricating the electrodes on the piezoelectric substrate, we use octadecyltrichlorosilane (OTS) to form the hydrophobic film on the substrate.[13] The trichlorosilane molecules are insulating, so they cannot be allowed to assemble on the electrodes. For this reason, the electrodes were first block by photoresist before the deposition of OTS. A lift-off procedure[14] is then used to remove the photoresist and OTS on the electrodes. The measured contact angle of 105° reveals that the surface of the substrate is very hydrophobic.

IV. RESULTS AND DISCUSSIONS

A. Moving droplets by a SFIT

Two 0.7-μl droplets, denoted by A_1 and B_1, are inserted on the propagation path of SAW. The frequencies with higher insertion loss of 70.1 and 66.5 MHz indicating the positions of droplets A_1 and B_1, respectively, as shown in Fig. 9(a). To move the droplet A_1, which was initially recorded at position of 70.1 MHz, we inputted a rf signal at 70.1 MHz and gradually increasing the electric power until the acoustic main beam has sufficient energy to drive the droplet. Pictures were taken in sequences to show the movement of the droplet A_1 with respect to the stationary droplet B_1 in Fig. 9(b). Meanwhile, we depict the simulated displacement field at 70.1 MHz in Fig. 9(c). It demonstrates that the amplitude at position A_1 is much greater than that at position B_1, and so only the droplet A_1 moved while B_1 remains stationary.

To further show that our design works with arbitrary droplets, we attempted to move the droplet on the left side with respect to the moved droplet A_1 at the right side. Similarly, two 0.1-μl droplets, denoted by A_2 and B_2, are placed on the path of the waves. The frequencies with higher insertion loss indicating the positions of A_2 and B_2 are recorded, as shown in Fig. 10(a). In this case, we inputted a signal of 65.6 MHz to move the droplet B_2. The motion of the droplet B_2 is observable, as shown in Fig. 10(b). We also simulated the displacement field at 65.6 MHz in Fig. 10(c) which indicates a remarkable agreement with the experiment. An interesting observation is that by comparing Fig. 9(b) with Fig. 10(b) we found that the velocity of the droplet B_2 is much slower than that of the droplet A_1. It is suspected that the insertion loss without droplets at 65.6 MHz is higher than that at 70.1 MHz in primitive frequency response so the acoustic power is smaller at 65.6 MHz.

B. Comparison of frequency responses between measurement and simulation

Figures 11(a) and 11(b) show the comparisons between measured and simulated results of frequency responses for detecting droplets using SFITs designed with different bandwidths. We assumed that the SAW excited by the SFIT propagates in a direction almost completely parallel to the bus bar. This assumption can be made since the tilt angles of the SFITs were designed to be less than 7°; thus the effects of beam steering could be neglected.[10] Hence, we can proceed to prove our simulation to be true by examining the frequency responses of our experiments and simulation. Therefore, we set the position of the droplet in simulation in the same position as that in the experiments; in other words, the frequency, which has maximum insertion loss in passband in the simulations, is equal to that in the experiments as the base of comparison. To constrain the width of the droplet base in simulation identical to that in the experiment, the micropipet was used to precisely control the volume of the droplets.

Although some deviations exist in the numerical results shown in Fig. 11, the frequency responses of simulations are quite similar to that of our measurements.

V. CONCLUSIONS

In this paper, we have proposed an effective method for simulating the performance of a SFIT, used for controlling the droplets. The numerical result of the amplitude profiles shows a good agreement with the movement of the droplets in experiment. We have also demonstrated how we can move different droplets by varying the driving frequency. In addition, a promising method is developed for the detection of the position of droplets through the analysis of frequency responses. In the future, this technique can be used to construct multichannel microfluidic chips which can manipulate droplets on a two-dimensional hydrophobic surface using two sets of SFITs, as shown in Fig. 12.

ACKNOWLEDGMENTS

The authors gratefully acknowledge the financial support from the National Science Council of Taiwan (Grant No. NSC 93-2218–E-002–052). The assistance of Z.-C. Hsu in editing the paper is also gratefully acknowledged.

[1] S. Shiokawa, Y. Matsui, and T. Ueda, Proc.-IEEE Ultrason. Symp. **1**, 643 (1989).
[2] T. Uchida, T. Suzuki, and S. Shiokawa, Proc.-IEEE Ultrason. Symp. **2**, 1081 (1995).
[3] A. Rathgeber, C. Strobl, H.-J. Kutschera, and A. Wixforth, *electronically found at*: http://arxiv.org/pdf/physics/0104079 (2002).
[4] C. J. Strobl, A. Rathgeber, A. Wixforth, C. Gauer, and J. Scriba,

Proc.-IEEE Ultrason. Symp. **1**, 255 (2002).
[5]H. Yatsuda, Proc.-IEEE Ultrason. Symp. **1**, 173 (2000).
[6]H. Yatsuda, S. Kamiseki, and T. Chiba, Proc.-IEEE Ultrason. Symp. **1**, 13 (2001).
[7]H. Yatsuda, K. Noguchi, and K. Yamanouchi, Jpn. J. Appl. Phys., Part 1 **39**, 3041 (2000).
[8]T.-T. Wu and Y.-Y. Chen, Chinese J. of Mechanics, series A 19, 225 (2003).
[9]Y.-Y. Chen, T.-T. Wu, and C.-T. Chou, J. Phys. D **37**, 120 (2004).
[10]T.-T. Wu and C.-M. Lin, J. Chin. Inst. Eng. **27**, 973 (2004).
[11]P. Dufilie, L. Kopp, J. V. Knuuttila, J. Vartiainen, and M. M. Salomaa, Proc.-IEEE Ultrason. Symp. **1**, 41 (2001).
[12]B. P. Abbott, Ph.D. dissertation, University of Central Florida, 1989.
[13]J. B. Brzoska, I. B. Azouz, and F. Rondelez, Langmuir **10**, 4367 (1994).
[14]D. Kleinfeld, K. H. Kahler, and P. E. Hockberger, J. Neurosci. **8**, 4098 (1988).